Optical Materials 121 (2021) 111511

Contents lists available at ScienceDirect

Optical Materials

journal homepage: www.elsevier.com/locate/optmat

Research Article

Enhanced thermal performance of photovoltaic panels based on glass surface texturization

Ángel Andueza [a,b,*], Cristina Pinto [c,a], David Navajas [a], Joaquín Sevilla [a,b]

[a] Dpto. Ing. Eléctrica, Electrónica y de Comunicación, Universidad Pública de Navarra, 31006, Pamplona, Spain
[b] Smart Cities Institute, Universidad Pública de Navarra, 31006, Pamplona, Spain
[c] National Renewable Energy Centre of Spain (CENER) Ciudad de La Innovación 7, 31621, Sarriguren, Spain

ARTICLE INFO

Keywords:
Radiative cooling
Photonic crystal
Glass surface texturization
Thermal radiation

ABSTRACT

Photovoltaic module temperature is a detrimental parameter influencing the energy yield and the durability of photovoltaic systems. Among the passive strategies to reduce the operating temperature of solar cells, radiative cooling is receiving a lot of attention, as an effective mean to passively evacuate heat in systems. The existence of a wavelength window of atmospheric transparency (8–13 μm) allows sending heat to outer space. The functionalization of the glass that could help to limit or reduce the temperature of the solar cells is an interesting approach. In this paper, we explore the effect of glass surface patterns in its radiation performance, so that the radiation cooling effect could be enhanced. The study is based on numerical simulations, calculating the spectral emissivity of different geometrical configurations of structures on top of the glass. Different geometrical figures of micrometers in size have been tested to find an optimal emissivity response in the transparent atmospheric window. Periodical patterns based on cones, pyramids, or moth-eye shapes result in emissivity responses close to one along thermal wavelengths (8–25 μm) which increases the emitted power of the glass. However, when assessing the cooling power under sunlight, the evaluation wavelength band has to be expanded (0.3–25 μm). Here, we found that not all geometrical figures are effective for radiative cooling. Surfaces textured by holes and pyramids show a substantial cooling effect, providing an increase in cooling power over the flat glass ranging from 40 W/m^2 to 110 W/m^2 depending on the temperature of the solar devices.

1. Introduction

The Earth's atmosphere is highly transparent in the 8-to-13 μm wavelength region. This transparency window matches the peak wavelength of the spectrum emitted by a blackbody at ambient temperature near 300 K. Moreover, the Universe at a temperature of 3 K represents a thermodynamic heat sink. Thus, any device at ambient temperature facing the sky dissipates heat emitting infrared thermal radiation into space [1]. This thermodynamic mechanism, called radiative cooling, is nowadays getting a lot of attention given its ability to passively cool without any extra energy input. To obtain the maximum benefit from this physical process, surfaces must be optimized so that their emittance is as high as possible in the atmospheric window.

Radiative cooling can be used for many applications and a lot of work is being done to allow its use in solar energy, specifically in photovoltaic solar cells. Absorbed sunlight is converted into electrical power by these devices, however, this absorption also increases its operating temperature worsening many of their characteristics, such as efficiency, open-circuit voltage, output electrical power or durability in the field. For crystalline silicon solar cells, the efficiency decreases by 0.5% for every ^{o}C of temperature increase [2]. To avoid this decrease in efficiency, the cell must be kept as cold as possible while assuring the absorption of all wavelengths useable for electricity production. For this purpose, radiative coolers are an interesting option, as far as they provide significant cooling power in the daytime.

Many materials and coatings have been investigated as thermal radiators. Historically, naturally available materials and synthetic polymers were first investigated for radiative cooling. Polyvinyl fluoride (PVF or Tedlar) was one of them, although it shows good cooling properties for night-time, at daytime, the response is not as good, not being appropriate for their use in solar cells [3,4]. Recently, new materials have been developed like metamaterials, multilayer coatings and photonic crystals (PC) which can provide more sophisticated thermal responses [5–9]. Zhu L. et al. [10] proposes a radiative cooler for solar

* Corresponding author. Dpto. Ing. Eléctrica, Electrónica y de Comunicación, Universidad Pública de Navarra, 31006, Pamplona, Spain.
E-mail address: angel.andueza@unavarra.es (Á. Andueza).

https://doi.org/10.1016/j.optmat.2021.111511
Received 15 June 2021; Received in revised form 19 August 2021; Accepted 21 August 2021
Available online 28 August 2021

absorbers compound in 2D silica photonic crystals, getting a decrease of 13 °C over the bare cell at noon. Other authors like Raman A. et al. [11] test 1D photonic crystal to act as an integrated photonic solar reflector and thermal emitter that reflects incident sunlight while emitting strongly and selectively in the atmospheric window, getting 4.9 °C below ambient temperature.

In this work, we explore the modification of the external surface of the protective glass that is employed as front cover in the photovoltaic modules to obtain the optimum thermal performance of the system. In order to operate at the lowest possible temperature, the emitted power from the panel surface (P_r in Fig. 1(a)) should be maximized. This emission is most effective in the atmospheric window of transparency (labeled B_{AW} in Fig. 1(b)), therefore the emissivity of the glass in this window should approach 1 as much as possible. On the other hand, the solar light useful to produce electricity in the solar cell (B_{VIS} in Fig. 1(b)) must traverse the glass with the minimum losses. Therefore, the ideal emissivity of the protective glass should change from cero to one at some point between both bands. This cutoff wavelength (W_{off} in Fig. 1(b)) has to be somewhere in the near-infrared band (B_{NIR} in the figure), and its precise position will affect the overall performance of the system.

Glass is a very good material for these purposes. It has a great response in the atmospheric window. It is transparent in the visible and near-infrared region (NIR), and in the mid-infrared region (MIR), it has very low reflectivity and high absorptivity/emissivity that allows becoming a great thermal emitter. However, the existence of phonon-polariton resonance in the 9 μm produces a peak of low absorptivity, therefore reducing the emissivity of the material. Moreover, the phonon-polariton resonance, shows a similar influence at 20 μm in the second transparent window can be significantly diminished by the patterning of 2D photonic crystals on the surface of the glass.

Many 2D photonic crystals on top of solar cells have been studied in the last decades with a different purpose. Diverse optical structures have been employed as anti-reflective surfaces in the visible range, such as pyramids [12,13], cylinders [14], domes [15], cones [16], moth-eyes [17], holes [18], etc. In most cases, the objective of these structures was to increase the transmitted optical power to the solar cell. Here we have revisited these structures intending to enhance the emissivity of the soda-lime glass in the atmospheric window. Besides, we have analyzed their performance in the whole spectrum so that we can propose a structure with the optimal daytime thermal performance without affecting transparency in the cell absorption band (B_{VIS}).

Glass is a well-known material, as it has been broadly used in construction for centuries and nowadays it is used in photovoltaic modules to provide rigidity and protection against atmospheric agents. So, to add these modifications on the surface there is no need to change the construction of the solar modules, just the addition of a small modification is needed to create the photonic structure that radiates into solar modules. Furthermore, the proposed structures are of the order of magnitude of the wavelengths analyzed, micrometers, so the fabrication of these can be done with processes, like optical lithography and reactive ion etching.

2. Structure design and simulacion

In this section, we describe the process followed to find glass surface periodic structures of high thermal performance. The first step is to perform series of simulations of different patterns changing shapes and sizes obtaining the spectral emissivity for all cases. Two different simulation tools had to be used, each suitable for one of the spectral bands of interest. These tools are described in detail in subsection 2.1.

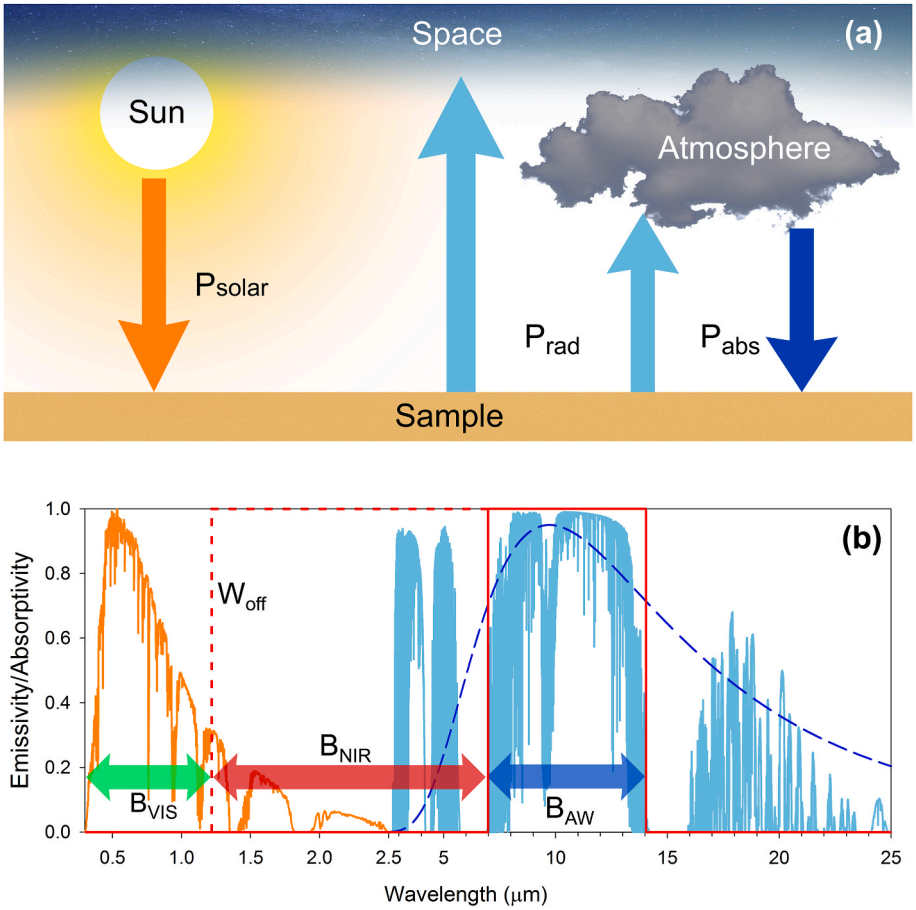

Fig. 1. Schematic diagram of (a) the radiative exchange of the surface of a photovoltaic panel and (b) the spectral intervals involved in the process.

Pattern shapes, sizes, and the systematic procedure to find the optimum are described in subsection 2.2. Finally, in order to obtain the actual thermal performance, we have to calculate the radiative power balance of the selected structures. These calculations require the integration of the spectral emissivity for different incidence angles as described in detail in section 2.3.

2.1. Simulation setup

To study the performance of an enhanced radiative cooling by tailoring glass surfaces with microstructures, we consider a 3D electromagnetic model of soda-lime glass. Simulations in thermal wavelength range were carried out using the CST MICROWAVE STUDIO™, a commercial code based on the Finite Integration time-domain Method (FIM) [19]. This program is an electromagnetic field simulation software package especially suited for analysis and design in the microwave, terahertz, and optical range.

In this work, a frequency solver with a tetrahedral adaptive mesh refinement was used to calculate the absorptivity of the textured glass in MIR region using a unit cell boundary condition with an infinite thickness in the glass (transversal electric field equal to zero). Therefore, we consider that the power transmitted through the glass is equal to zero, and the incident power is divided into reflected and absorbed power. That previous condition is considered to model the fact that the real thickness of the glass (3.2 mm) is much larger than the infrared (IR) wavelength range (8–25 μm) corresponding to atmospheric transparent windows.

To compare and analyze total IR light absorption enhancement in the transparent window, a soda-lime glass layer was considered, as is shown in Fig. 2. It corresponds to a bulk glass film tailored by a regular pattern of microstructures. In all cases analyzed, we considered a square unit cell to perform the numerical calculations due to the geometry is most stable and simple to fabricate than the triangular one. As is depicted in Fig. 2, in the following, we will refer to the plane containing the microstructures as *xy*, being z the incidence radiation axis of the Transverse Electric and Magnetic (TEM) excitation mode. The separation between centers of the microstructures, or pitch, is denoted by ***a***, being ***r,*** and ***h*** the radius and height of the microstructures on the top of the glass layer, respectively. In the simulations, we consider a finite thickness ***d*** in the glass layer before applying the boundary condition of tangential electric field zero. This value ***d*** was determined by simulation to guarantee that results presented are similar to those obtained in the case of simulating an infinite thickness. The combination of this finite thickness and null boundary condition of the tangential electric field reduces the convergence time of the simulation at the same time that achieves accurate results [20].

The meshing method employed by CST to calculate the absorption depends on the dimension of the unit cell concerning the shorter wavelength of the simulation. This fact implies that necessary meshing for simulating the microstructures in the visible range exceeds the capacities of any computer. For that reason, to analyze the absorptivity response in the visible and NIR range, we employ Grating Diffraction Calculator (GD-Calc) [21], a software package developed by Kenneth C. Johnson and implemented entirely in MATLAB that uses rigorously coupled-wave analysis (RCWA) [22]. GD-Calc solves the Maxwell equations for a single frequency and analyzes the weight of each diffraction order separately. A summation of the power density in all diffraction orders provides the reflection, R, and transmission, T, obtaining Absorption as A = 1 - R - T. The unit cell geometry in GD-Calc is made out of discrete rectangular bricks arranged in strata which are divided into lateral stripes and subdivided into blocks to fill 3D space up. GD-Calc resolves the meshing problems of CST since is possible to simulate structures much larger than the shorter wavelength of the calculation [23].

The soda-lime glass is transparent in the visible range and has a refractive index almost constant of 1.4. However, it presents a refractive index significantly different in the region of the IR corresponding to the atmospheric windows between 8 and 20 μm; soda-lime glass behaves as high absorbent material from 4 μm where the power transmitted can be considered null. This electromagnetic behavior of soda-lime glass in the IR range has been previously studied and analyzed by the scientific community. In this paper, we will employ refractive index data of soda-

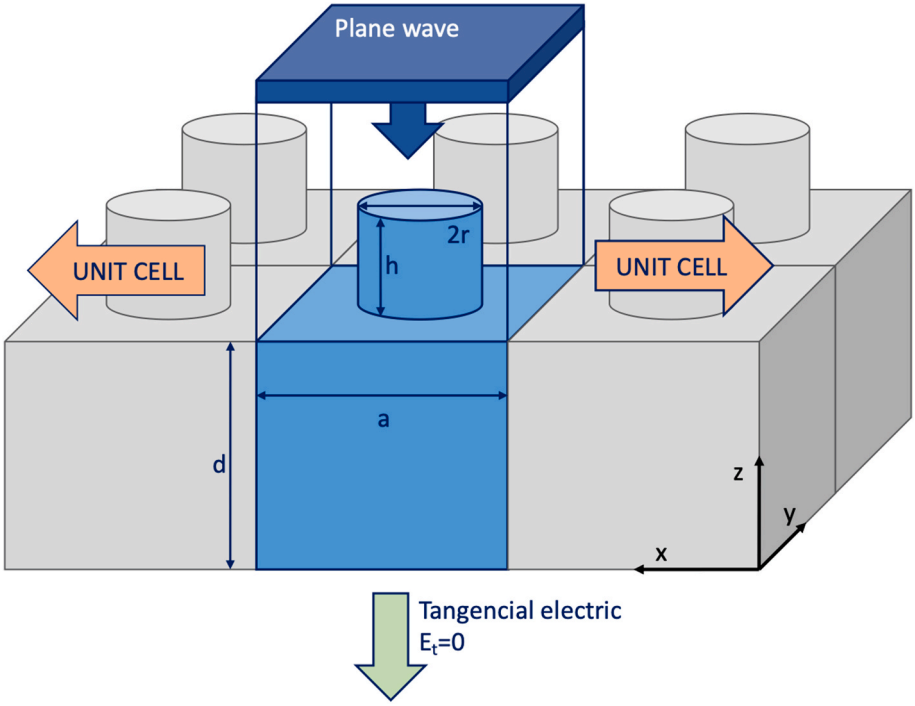

Fig. 2. Sketch of a structured array of square microcylinders of radius r, height h, and pitch a, on the top of a silica bulk layer of thickness *d*. The axis and boundary conditions employed in the simulation are also depicted in the plot.

lime glass from Rubin [24] to simulate the electromagnetic behavior shown by the proposed microstructures.

2.2. Optimization of the simulated nanostuctures

Radiation impinging a surface splits into three components: reflected, transmitted, and absorbed. Due to the optical properties of the soda-lime glass (as indicated by its refractive index) there is no transmitted radiation in the atmospheric transparency window, all is absorbed as traversing the glass. Thus, if we want to enhance the emissivity (absorptivity) of the radiator, we must modify the ratio between reflected and absorbed power. A flat surface of glass can reflect until 21% of MIR incident power, absorbing around 79%. Therefore, by creating IR antireflective structures on the radiator surface, the power reflected can be substantially reduced obtaining a high emissivity response. Therefore, to characterize and compare the performance of each structure, we use the average emissivity ε_r, calculated as the integral of the absorptivity spectrum over the thermal wavelength range (8–13 μm). A perfect absorptivity in this window corresponds to 1.

Among the huge diversity of possible patterns, we have limited our study to a set of basic geometries: cylinders, cones, cylinder holes, moth-eyes, domes and pyramids. For each one of these structures, we have to optimize the geometrical parameters that define them: the pitch (***a***), the radius or base size (***r***), and the height (***h***). It is important to note that two parameters (***r*** and ***a***) are mutually dependent determine the other one. Once the variables that must be taken into account have been identified, we must define a range of variations according to generate a significant response at the transparency window and the limits in the fabrication process. The height (***h***), in most cases, is limited by the technique employed in the fabrication. For that reason, we have selected two values to define the upper and lower limit of designing. The upper and lower limits have been set at 10 μm and 0.2 μm, respectively. In the case of pitch (***a***) has been defined between 2 and 8 μm to increase the influence of the structure in the absorption process generated by the structure. Besides, these values are typical in the fabrication process based on ultraviolet (UV)-photolithography and reactive ion etching techniques. Finally, in the case of the structure radius (***r***), the limits are given by the value of pitch and the fabrication process employed. For that reason, we have selected a range of variations far away from the maximum and minimum values imposed by the pitch. The lower and upper reasonable values are 10% and 50% of pitch values, respectively. Therefore, we have defined the range of variation of the radius between 0.4 and 4 μm. The reason of select an upper radius value of 4 μm is to evaluate the performance of the textured surfaces in close-packed configurations.

From these three geometrical parameters that define the structures and their variation ranges, we can define a 3-level central composite design (CCD) to obtain an optimized absorptivity response without a large number of simulations [25]. For the cases of three variables, we have to simulate 15 combinations of the parameters under study (pitch, radius, and height). This process does not consider the mutual dependence that exists between radius and pitch which can generate unfeasible structures. The simulations where the radius is larger than half-pitch will be treated as flat glass. The existence of these empty simulations implies a loss of information in the process of determining the optimized absorptivity response. For that reason, in the most promising structure, it has been performed a second sweep with its central point in the optimum obtained in the first one and with a smaller variation of the parameters to avoid overlapping between them.

2.3. Evaluation of radiative power

In order to evaluate the actual thermal performance of glass textured with different patterns, we need to calculate the radiative power balance of the system. A general view of the radiative processes involved can be seen in Fig. 1(a). The emitted radiation from the surface of our glass will partially leave through the earth's atmosphere to space which works as an infinite sink of heat at 4 K [26]. Another part of this radiation will be trapped by the surrounding atmosphere and will also receive radiation from it.

The heat exchange processes will depend on different factors, such as conductive and convective heat gain due to the sun or wind movements. We will have to consider a homogeneous situation for the comparison of different textured surfaces. To do so, let's start by stating the power balance of the system as

$$P_{net} = P_r - P_a - P_{sun} - P_{nr} \tag{1}$$

where

$$P_r = 2\pi \int_0^{\pi/2} sin\theta cos\theta d\theta \int_0^{\infty} B(T_r,\lambda)\varepsilon_r(\lambda,\theta)d\lambda \tag{2}$$

P_r is the radiative power emitted by the radiator and

$$P_a = 2\pi \int_0^{\pi/2} sin\theta cos\theta d\theta \int_0^{\infty} B(T_a,\lambda)\varepsilon_a(\lambda,\theta)\varepsilon_r(\lambda,\theta)d\lambda \tag{3}$$

is the incident atmospheric thermal radiation which is absorbed.

P_{sun} is the absorbed solar power by the radiator.

$$P_{sun} = 2\pi \int_0^{\infty} \varepsilon_r(\lambda,\theta_{sun})B_{solar}(\lambda)d\lambda \tag{4}$$

The solar power term must be considered to estimate the radiative cooling efficiency during the daytime. The last term of the right-hand side of Equation (1) P_{nr} is the absorbed non-radiative power from surrounding, which can be defined as

$$P_{nr} = h_c(T_a - T_r) \tag{5}$$

where, h_c is the combined conduction and convection heat transfer coefficient. This term includes conduction and convection and will be mostly affected by the weather conditions at each time. As we are interested in the radiative balance, so that we can optimize the glass pattern for this purpose, we will assume the same value of P_{nr} for all of them. Therefore, from now on, and always for comparison purposes, we do not consider this term.

The black body radiation according to Planks law at any temperature is

$$B(T,\lambda) = \frac{2hc^2}{\lambda^5}\frac{1}{e^{hc/\lambda kT} - 1} \tag{6}$$

where h is the Plank's constant, k es the Boltzman constant, c is the speed of the light, λ the wavelength and T is the temperature. In equations (2) and (3), ε_r and ε_a are the emissivity/absorptivity of the radiator and atmosphere, respectively. Note that, emissivity can be defined by absorptivity according to Kirchhoff's law. The directional emissivity of the atmosphere $\varepsilon_a(\lambda,\theta)$ is calculated as $\varepsilon_a(\lambda,\theta) = 1 - t(\lambda)^{1/cos\theta}$ where $t(\lambda)$ is the atmospheric transmittance in the zenith direction. The atmospheric transmittance depends on the column water vapor and air mass value. In this work, the column water vapor and air mass are assumed to be 10.0 mm and 1.5, respectively [27]. T_r is the temperature of the radiator and T_a es the ambient temperature. In equation (4), we define B_{solar} as the incident solar irradiation and θ_{sun} as the zenith angle between the sun and the vertical of the radiator. Solar irradiance employed was obtained by SMARTS (Simple Model of the Atmospheric Radiative Transfer of Sunshine) code at mid-latitude conditions [28].

According to equation (1), a radiator will generate an effective cooling only when the radiated output power exceeds the total absorbed power, resulting in a net cooling power P_{net} positive. For an optimal operation, absorbed power from the sun and the incoming atmospheric

radiation has to be minimized or limited, and emitted power in the transparent window spectrum, has to be maximized. This strategy has as result a radiator temperature (T_r) lower than the atmosphere temperature (T_a) [26]. Thus, according to equation (2), the performance of the proposed system is highly dependent on the spectral emissivity profile of the radiator, in our case, soda-lime glass. For solar cell applications where the device itself produces a lot of heat or gains a lot of heat from the sun, the glass layer temperature can show an important increase of temperature, and corresponding nominal module operating temperature (NMOT) of approximately 45 °C can be found in module datasheets. Therefore, in our study case, radiative cooling below the ambient temperature may not be possible at daytime conditions. In such a case, a glass radiator can be useful to decrease the device temperature rather than cooling it below the ambient temperature.

3. Results and discussion

In order to conclude which is the best surface texturization of glass to increase radiative cooling, we have analyzed several characteristics as follows: first, we optimize the size of each of the selected motifs to obtain the highest emissivity under incident radiation in the atmospheric window. Then we present the angular variation of this emissivity (section 3.1). Afterward, we perform a sensitivity analysis to assure that the optimum emissivity dependence with the dimensions is compatible with typical fabrication tolerances (section 3.2). Finally, in section 3.3 we present the daylight power balance of each structure, which includes the evaluation over a wider spectrum: visible, NIR and atmospheric windows.

3.1. Optical analysis of optimized microstructures in silica

In this section, we will analyze and compare different patterns in the surface of a layer of soda-lime glass that presents a thickness larger than the wavelength of the IR light in the atmospheric window. As previously stated, the motifs under study include cylinders, cones, cylinder holes, moth-eyes, domes and pyramids. The dimensions of each microstructure have been optimized to maximize the average emissivity in the 8–13 μm band as described in section 2.2.

Table 1 summarizes the values of the geometrical parameters obtained for each optimized structure derived by the design of experiments (DOE) process. From here on out, the presented results will correspond to the optimal configuration of each geometry analyzed. As previously stated, we employ average emissivity $\boldsymbol{\varepsilon_r}$ (the integral of the absorptivity spectrum in the wavelength range 8–13 μm) to characterize and compare the performance of different structures. The result of each structure is presented in the last column of Table 1.

Fig. 3 shows emissivity spectra of flat and structured glass surfaces, respectively. Calculated absorptivity is always presented averaged over both polarizations, TE and TM, at normal incidence. In Fig. 3 the broad peak at 9 μm in the emissivity spectrum of flat glass is clearly shown. In contrast, placing textured patterns on top of the glass result in a significant decrease of this peak, somehow different for each of the considered geometrical motifs.

It is important to note that all the structures provide a significant

Table 1
Summary of geometrical parameters and average emissivity in the transparent window for each optimal configuration analyzed.

Structure	Pitch (μm)	Radius (μm)	height (μm)	Average emissivity (ε_r)
Flat glass	-	-	-	*0.79*
Cylinders	*5.39*	*1.61*	*2.20*	*0.98*
Cones	*5.00*	*2.50*	*10.00*	*0.99*
Holes	*6.12*	*3.00*	*2.54*	*0.98*
Moth-eye	*5.00*	*2.50*	*10.00*	*0.99*
Domes	*6.86*	*2.71*	*2.71*	*0.97*
Pyramids	*5.00*	*2.50*	*10.00*	*0.99*

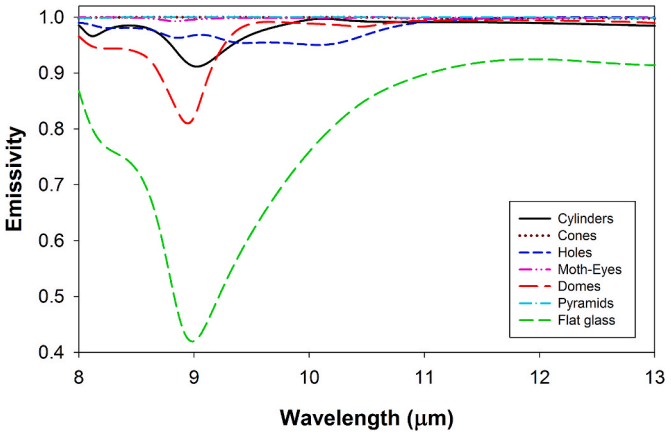

Fig. 3. Emissivity spectra of a flat glass sample (blue line) and optimized structured samples of cylinders (solid black line), cones (dotted brown line), holes (short-dashed blue line), moth-eye (double dash-dotted pink line), domes (long-dashed red line) and pyramids (dash-dotted cyan line), respectively. The calculations were carried out at normal incidence with infinite glass thickness. Emissivity is presented averaged over both polarizations, TE and TM.

increase in the absorptivity spectrum, larger than 18% concerning flat glass. Domes appear as the structure with worse enhancement performance but only around 3% lower than the other ones. The peak of flat glass at 9 μm remains noticeable in the emission spectrum of domes, generating a penalty in the final performance. However, cones, moth-eye, and pyramids are the best structures since their emissivity curves are overlapping close to 1, as is shown in Fig. 2. The $\boldsymbol{\varepsilon_r}$ value in all structures is almost 1. Finally, cylinders and holes also present a very good emissivity performance of 0.980 and 0.981, respectively but slightly worse than cones, moth-eye, and pyramids structures. In Fig. 3, we can see a marked difference between both structures at 9 μm; cylinders maintain the presence of the peak however, holes present a flat and smooth absorption around 0.96 where the peak is almost imperceptible. Therefore, cylinders and domes are less efficient because of a worse performance to remove the peak in the absorption spectrum of the glass.

It is not surprising that all texturing patterns perform significantly better than flat glass because the texturing decreases the reflectivity of the surface. In the infrared range considered the glass absorptivity is so high that no power is transmitted (T = 0). Therefore all incoming power is either reflected or absorbed (R + A = 1), converting the problem from increasing emissivity to reducing reflectivity.

Strategies to do so include: (i) increasing the effective surface of the geometrical sample (increase roughness), (ii) changing the incidence angles so that part of the reflected light can hit the surface at other glass point and (iii) make a smooth refractive index transition between air and solid glass (introducing a gradient of the filling factor of glass with depth). These effects are best achieved by pyramids, cones and moth-eye (especially (ii) and (iii)) and holes (effects (i) and (ii) mainly). Besides, this reflectivity decrease has to be obtained in the infrared region, so the size of the texturing structure has to be comparable to the wavelength of this radiation.

The radiative exchange of a surface and its environment takes place in all directions; therefore, it depends on the emissivity for each incident angle, as can be seen in its mathematical description, given by equation (2) (section 2.3). Thus, textured structures on the top of the glass must be able to maintain a near-unity absorption response independently of the incidence angle of the radiation. Previous results in Fig. 3 took only into account the response at normal incidence. Fig. 4 shows the directional average emissivity $\boldsymbol{\varepsilon_r}$ in the 8–13 μm range for all the structures compared to that of flat glass.

The emissivity of the textured samples is more than 0.80 in most angles, only decreasing for angles larger than 60°. In all cases, the

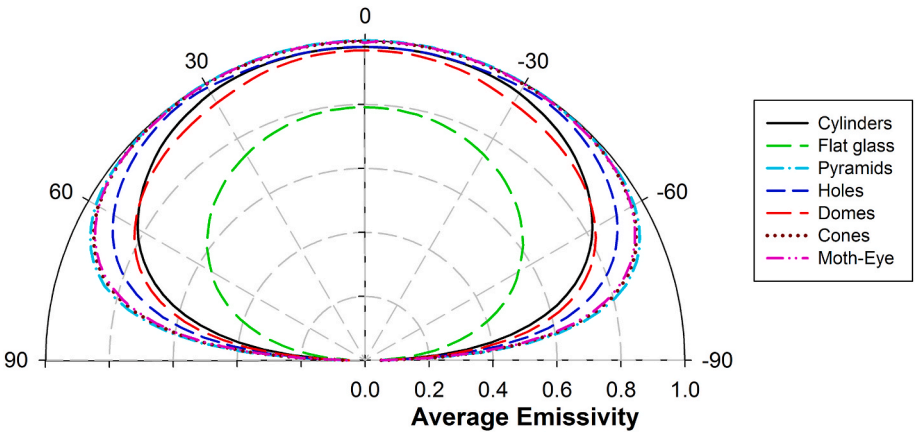

Fig. 4. Average emissivity in the transparency window (8–13 μm) as a function of angle of incidence of a flat (green dashed line) and structured glass layers of cylinders (solid black line), cones (dotted brown line), holes (short-dashed blue line), moth-eye (double dash-dotted pink line), domes (long-dashed red line) and pyramids (dash-dotted cyan line), respectively. Emissivity is presented averaged over both polarizations, TE and TM.

emissivity of textured glass samples is higher than flat glass ones, with an average emissivity enhancement between 20% (for small angles) and almost 60% (angles larger than 60°). Cones, moth-eye, and pyramids maintain close to unity even near incident angles larger than 60°. The emissivity ε_r in the 8–13 μm spectrum for these structures is 0.965, 0.960 and 0.970, respectively, which only suppose a decrease of 3% regarding normal incidence. This result indicates that cone, moth-eye and pyramids present an emissivity response slightly dependent on the incidence angle of light and close to unity in large angles. The rest of the structures, cylinders, domes and holes, present good emissivity results close to 60° but always under the values shown by the best structures. Therefore, the previous result is a good feature to maximize the radiated power (P_{rad}) according to equation (2) and show that the microstructures on top of glass have desirable properties for daytime radiative cooling.

The best structures in the atmospheric transparency window present a strong influence from their height. Cones, moth-eye and pyramids have an aspect ratio (defined as $\boldsymbol{h/2r}$) of 2, far away from the value presented by the other structures, around 0.5. A high aspect ratio assists to reduce the reflectance and increase the total emissivity of the glass in 8–13 μm range.

We can regard all these structures as a way to smoothen the refractive index change suffered by the incident light when passing from air to glass, providing effective impedance matching between glass and air over a broad range of wavelengths. Therefore, the steeper transition of refractive index that appears between air and glass substrate in cylinders and holes, produces a worse reflectance compared to textured surfaces with a more gradual index profile. Furthermore, this behavior is even clear when light impinges obliquely, as was demonstrated in Fig. 4.

3.2. Tolerance of optimized structures to fabrication errors

We want to determine if the optimum sizes previously found require very precise values or, on the contrary, the performance does not degrade quickly as sizes depart from their optimal values. So, we have checked the emissivity of the structures for different values of their sizes close to the optimal ones. In order to provide a quantitative assessment of these variations we use standard fabrication tolerances for size variations and evaluate its tolerance to fabrication errors based on a worst-case tolerance analysis [29], where the individual variables of fabrication are placed at their tolerance limits to make the emissivity calculation as large or as small as possible. This model predicts the maximum expected variation of the measurement of the errors in design variables. For this analysis, we applied a variation around the optimal variables of design of ±5%, which is coherent with the expected errors that can be produced during the usual manufacturing processes of 2D textured surfaces in glass. A total of 27 combinations of tolerance limits have been simulated (not considering unfeasible structures). Afterward, the emissivity response performance is assessed for each case.

The tolerance analysis shows that the maximum emissivity standard deviation obtained for all the structures, never exceeds 1.3%, as can be seen summarized in Table 2. From these results, we can conclude that the proposed textured structures in glass are not significantly sensitive to small errors during the fabrication processes and therefore the emissivity response is robust.

3.3. Radiative cooling power balance of the structures under sunlight

Previous subsections of this paper have been devoted to optimizing the average emissivity between 8 μm and 13 μm, the atmosphere transparent window. However, when the structure is facing the sun, which emits in other infrared windows as well as visible, further analysis is needed. In the following, we evaluate the net radiative cooling balance for the analyzed structures in the whole visible-IR spectrum, evaluating their performance regarding the absorption of atmospheric and solar thermal radiation.

The following assumptions have been made in this section: first, since the radiative cooling has been evaluated in mid-latitude zone, we assume a typical ambient temperature $T_a = 25$ °C (298 K). Second, we calculate the cooling power of the structures without non-radiative heat transfer ($h_c = 0$) to estimate exclusively the effect of radiated power by the glass. The spectral transmittance of the atmosphere and the AM1.5 solar radiance employed in the calculations were indicated in section 2.3.

To evaluate the net cooling performance of our textured surfaces and the pondered weight of each power term in equation (2), we first perform net power calculations where radiator temperature T_r and ambient temperature T_a, are equal. The results are presented in Fig. 5. The emitted power by the surfaces (P_{rad}) does not change much as the structure varies, and it moves between 320 W/m^2 and 356 W/m^2, and

Table 2
Statistics of worst-case tolerance distribution in each structure.

Structure	Average emissivity (ε_r)	Standard deviation σ (%)	Maximum emissivity deviations (%)
Cylinders	*0.978*	*0.19*	*0.83*
Cones	*0.997*	*0.12*	*1.3*
Cylinder holes	*0.978*	*0.65*	*1.3*
Moth-eye	*0.997*	*0.04*	*0.13*
Domes	*0.967*	*0.32*	*1.2*
Pyramids	*0.999*	*0.06*	*0.05*

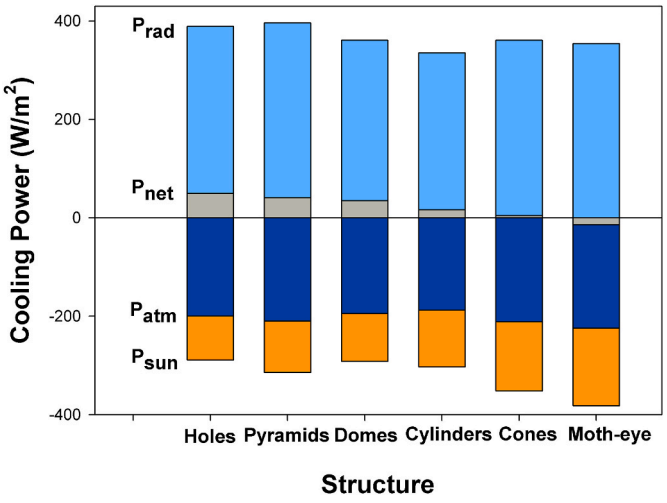

Fig. 5. Distribution of net cooling power (grey), radiated (lightSkyBlue) and absorbed (blue and orange) power for each optimized structure when ambient and radiator temperatures are equal. The color of the bars is correlated with the previous Fig. 1.

the best result corresponds to the structures with the best performance in the transparent window: cones, moth-eye and pyramids.

The absorbed power by the structured glass from the atmosphere (P_{atm}) maintains almost constant since P_{atm} is mainly influenced by the radiative properties in the infrared range from 4 μm to 25 μm, and the absorptivity response of the structures at long wavelength remaining near to 1 in all cases. On the other hand, the absorbed power from the sun P_{sun}, mainly produced by the absorption in the solar spectrum (0.3–1 μm), varies significantly among the studied structures. Moth-eye structure is the most sensitive to solar absorption (158 W/m^2) while holes absorb the least solar energy (89 W/m^2). Note that not all the structures present a positive net cooling power at daytime since moth-eye is heated under these temperature conditions at daytime.

As we have seen, cooling performance is poor for moth-eye and cones structures with lower P_{net} values than holes and pyramids. However, these structures presented similar emissivity performance in the transparent window. Therefore moth-eye and cones must have worse emissivity responses in the visible (0.3–7.5 μm) range. To go into detail about this behavior, we present in Fig. 6 the emissivity spectra of flat and structured glass in a wide spectrum.

For the uniform flat glass layer, the emissivity shows two large dips that correspond to the photon-polariton resonances of silica. The dips are located at the atmospheric window and a secondary low transmission window from 20 to 25 μm. Moreover, both windows coincide with the range of blackbody radiation at ambient temperature (300 K) and determine the contribution of radiated power and absorbed atmospheric power by the radiator. All glass texturizations showed in Fig. 6(a), present an emissivity very close to unity at the whole range of thermal wavelengths (4–25 μm). The optimization process has eliminated the two peaks at 10 and 20 μm from absorptivity spectra in moth-eye, cones and pyramids structures, but remains at 20 μm for the glass textured with holes.

On the other hand, the absorptivity of the samples is quite different for wavelengths under 4 μm. First, only the textured glass with holes presents an absorptivity similar to flat glass for visible and NIR ranges. Pyramids increase slightly the absorption between 2.5 μm and 4 μm with respect to flat glass, but cones and moth-eye do it especially in the visible wavelengths. This increase in the absorptivity is traduced in a gain in the solar power that ruins the net power balance of glass.

More details can be seen in the optical spectrum from 0.3 μm to 1 μm is shown in Fig. 6(b). The average emissivity in 0.4–1 μm range for the glass is 4.7%. The emissivity shown by cones and moth-eye is much larger than reference glass, with values of 8.3 and 9.6%, respectively. So, a higher solar power will be absorbed by these structures and P_{sun} term will be significantly increased being very important for daytime cooling. The rest of the structures present quite similar emissivity spectra to flat glass, such as holes (4.9%), domes (5.4%), pyramids (5.8%) and cylinders (6.6%) and the net cooling power remains positive as shown in Fig. 4.

Previous calculations were performed with equal values of radiator T_r and ambient T_a temperatures. Now we present the cooling power performance of each optimized structure as a function of temperature difference. The power balance is shown in Fig. 7 as a differential value between the net cooling power of each textured glass sample and the reference flat glass. It is important to note that nonradiative power does not depend on the emissivity of the glass and its contribution in the flat or structured glass will be canceled in the differential power balance plotted.

As the radiating surface increases its temperature (T_r) the amount of radiation it generates changes according to equation (2), where the total power is obtained by integrating the blackbody radiation (equation (6)) multiplied by its emissivity, which depends on wavelength and angle. For all surfaces, as the temperature increases so does the blackbody radiation and therefore the total emitted power. However, this increase is not linear and depends on surface patterning. In addition, the atmospheric and solar absorption is different for each surface texturing (Fig. 6 (b)), and strongly dependent on ambient temperature and incident solar irradiation, respectively. All these effects together lead to the result shown in Fig. 7.

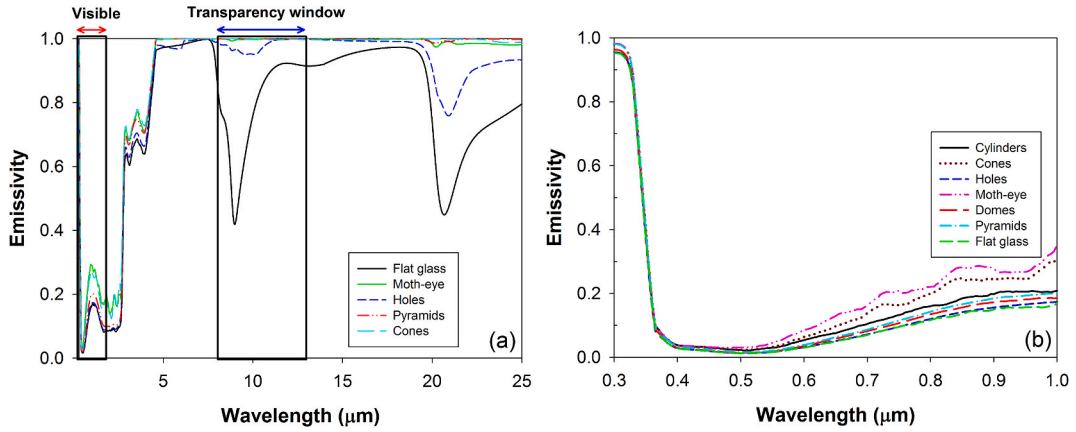

Fig. 6. Absorptivity simulation results of several structures of soda-lime glass with a thickness of 3.2 mm at normal incidence from 0.3 to 25 μm (b) Detail of absorptivity for the optimized structures in the visible range (0.3–1 μm).

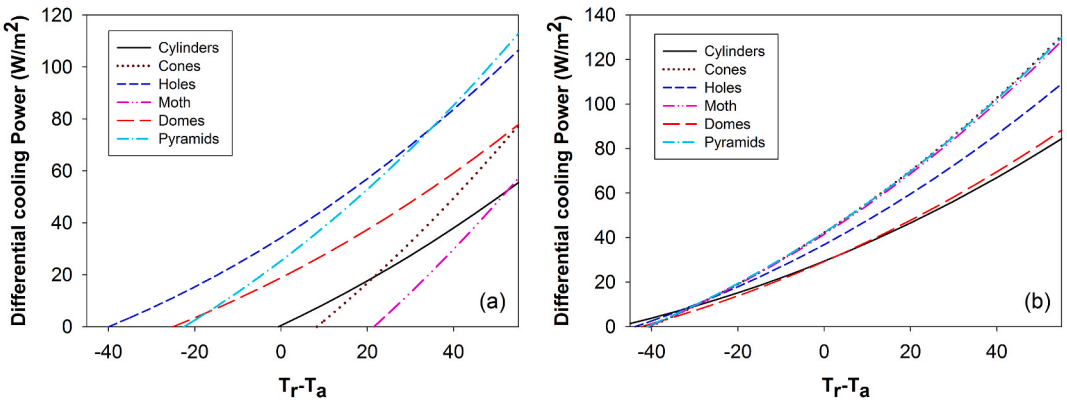

Fig. 7. Differential cooling power as a function of temperature difference for structures on the top of the glass (a) under direct sunlight (AM1.5) and (b) at nighttime. Ambient temperature is assumed to 298.13 K.

The first thing to notice about differential cooling power at daytime is that not all the structures present net cooling power better than flat glass; only pyramids, holes and domes have a positive value of differential power balance for radiator temperature lower than ambient. The structures based on cones, cylinders and moth-eye start to be better than glass at 0, 8 and 22 °C under ambient temperature, respectively. Besides, the cooling power performance obtained by them is always lower than pyramids or holes. The poor performance for these structures arises from the increased absorption of solar power previously studied.

When the cooler sample glass and ambient temperatures are the same, holes can achieve a cooling power of around 34 W/m^2 over the glass value. Holes show the best cooling performance of power with a power gain of 106 W/m^2 at 55 °C under T_a. The cooling power of pyramids becomes better than holes with increasing T_r and achieves a value larger than 113 W/m^2 at 55 °C under the ambient temperature. The behavior previously described for the cooling power for holes and pyramids arises from Kirchoff's law. A higher emissivity value increases the total thermal radiation absorbed (P_a) by the glass under the same ambient temperature. Then, if the temperature of the radiator is low and close to ambient temperature (T_a), the radiated power is partially compensated (P_r) by thermal absorption (P_a), and the net cooling power obtained is substantially reduced. In the case of pyramids and holes, the higher emissivity of the pyramids increases the weight of radiated power but also solar and thermal absorbed power. This effect makes that only when the temperature of the radiator is high enough, the net power balance is better than the holes. This result is especially important depending on the particular solar cell application because the operating temperature of solar cells in outdoor conditions ranges around 50–60 °C with values that can reach until 80 °C in the worst conditions. Therefore, it could be possible to obtain an enhancement between 60 and 75 W/m^2 at daytime in solar panels only by texturing surfaces with holes and pyramids.

At nighttime, all the considered radiator structures present a cooling power better than glass, even with a radiator temperature 45 °C below the ambient. Pyramids and cones present the best performance of cooling power regarding glass, which is more than 40 W/m^2 at the ambient temperature, and achieve until 130 W/m^2 with a temperature 55 °C higher than ambient, as shown in Fig. 7(b). Holes do not offer optimal performance at nighttime since their emissivity is lower than cones and pyramids in the transparency window and therefore the radiated power is lower. Without the direct sunlight influence, the negative effect undergoes by moth-eye glass surfaces due to the solar absorbed power is attenuated and obtains a similar performance than cones and pyramids.

Now that we understand the features of textured glass surfaces as radiators, we can conclude that the best structure to operate in high radiator temperature, as in the case of solar cells, are the pyramids since combines simultaneously a good performance at daytime and nighttime from 15 °C above ambient temperature. However, holes have larger cooling power than pyramids until temperatures 35 °C above ambient at daytime that compensate their lower cooling power at nighttime. This fact, make holes an ideal radiator for temperatures around or lower than ambient.

4. Conclusions

In this work, we have studied the periodic texturization of glass to enhance its properties for radiative passive cooling, particularly in photovoltaic devices. Six different types of 2D glass structures (cones, cylinders, domes, holes, moth-eye, and domes) have been optimized and compared to evaluate their performance as passive coolers. In order to find the optimum dimensions for each pattern geometry providing the highest emissivity spectrum in the atmospheric transparency window, a computer optimization procedure was performed. The textured glass surfaces based on pyramids, cones and moth-eye had better emissivity responses than the rest of the structures considered in this work and achieved near-unity emissivity in the desired band (8 μm–13 μm).

The cooling power of all the structures was calculated for daytime conditions, over the extended wavelength range (0.3–25 μm) including the sun emission and the atmospheric transparency windows. The cooling power achieved by the holes and pyramids structures is substantially improved, with respect to standard flat glass, with a radiative cooling power of 70 W/m^2 at 30 °C above the ambient temperature. However, cones and moth-eye glass structures presented a larger emissivity regarding glass in the visible and near-infrared ranges that increased the solar power absorbed at daytime, and the resulting cooling power decreased by 30 and 60 W/m^2, respectively. These results make these structures useless during daytime operation.

Therefore we conclude that only holes and pyramids are suitable candidates as glass surface texturing for radiative cooling applications in solar panels. Pyramids are better coolers for operation temperature by at least 15 °C above ambient temperature when the radiator is used to decrease the device temperature. On the other hand, holes present their best cooling performance around or lower ambient temperature and can be more useful for cooling the device below the ambient. This enhancement of cooling power makes it an interesting tool to improve the efficiency and performance of any solar cell only by using superficial textured glass on the top layer.

CRediT authorship contribution statement

Ángel Andueza: Conceptualization, Methodology, Software, Writing – original draft. **Cristina Pinto:** Data curation, Resources, and Software. **David Navajas:** Visualization, Software. **Joaquín Sevilla:** Conceptualization, Writing- Reviewing and supervision Editing.

Declaration of competing interest

The authors declare that they have no known competing financial interests or personal relationships that could have appeared to influence the work reported in this paper.

Acknowledgments

This work has been partially supported from Departamento de Universidad, Innovación y Transformación Digital de Navarra via Project PC036-037, DESAFIO, DEsarrollo de eStructurAs FotónIcas para aplicaciones fOtovoltaicas.

Cristina Pinto gratefully acknowledges the Department of University, Innovation and Digital Transformation of the Government of Navarra for the grants for hiring doctoral students and doctoral students by companies, research centres and technology centres: Industrial Doctorates 2020, with file number 0011-1408-2020-000003, received to carry out this work.

References

[1] W. Li, S. Fan, Radiative cooling: harvesting the coldness of the Universe, Opt Photon. News 30 (2019) 32, https://doi.org/10.1364/OPN.30.11.000032.
[2] E. Skoplaki, J.A. Palyvos, On the temperature dependence of photovoltaic module electrical performance: a review of efficiency/power correlations, Sol. Energy 83 (2009) 614–624, https://doi.org/10.1016/J.SOLENER.2008.10.008.
[3] D. Zhao, A. Aili, Y. Zhai, S. Xu, G. Tan, X. Yin, R. Yang, Radiative sky cooling: fundamental principles, materials, and applications, Appl. Phys. Rev. 6 (2019), 021306, https://doi.org/10.1063/1.5087281.
[4] S. Catalanotti, V. Cuomo, G. Piro, D. Ruggi, V. Silvestrini, G. Troise, The radiative cooling of selective surfaces, Sol. Energy 17 (1975) 83–89, https://doi.org/10.1016/0038-092X(75)90062-6.
[5] M. Hussein, M.F.O. Hameed, N.F.F. Areed, S.S.A. Obayya, Ultra-high efficient solar cell based on decagonal arrays of silicon nanowires, Opt. Eng. 53 (2014), 117105, https://doi.org/10.1117/1.OE.53.11.117105.
[6] M. Florescu, H. Lee, I. Puscasu, M. Pralle, L. Florescu, D.Z. Ting, J.P. Dowling, Improving solar cell efficiency using photonic band-gap materials, Sol. Energy Mater. Sol. Cells 91 (2007) 1599–1610, https://doi.org/10.1016/J.SOLMAT.2007.05.001.
[7] M.M. Hossain, B. Jia, M. Gu, A metamaterial emitter for highly efficient radiative cooling, Adv. Opt. Mater. 3 (2015) 1047–1051, https://doi.org/10.1002/adom.201500119.
[8] H. Bao, C. Yan, B. Wang, X. Fang, C.Y. Zhao, X. Ruan, Double-layer nanoparticle-based coatings for efficient terrestrial radiative cooling, Sol. Energy Mater. Sol. Cells 168 (2017) 78–84, https://doi.org/10.1016/J.SOLMAT.2017.04.020.
[9] Cuilian Xu, Shaobo Qu, Mingbao Yan, J. Zhang, W. Wang, Jiafu Wang, Yongqiang Pang, Yongfeng Li, Hua Ma, Design of the infrared selective thermal radiation based on metamaterials, Prog. Electromagn. Res. Symp., IEEE, 2016, pp. 2735–2738, https://doi.org/10.1109/PIERS.2016.7735113.
[10] L. Zhu, A.P. Raman, S. Fan, Radiative cooling of solar absorbers using a visibly transparent photonic crystal thermal blackbody, Proc. Natl. Acad. Sci. U. S. A. 112 (2015) 12282–12287, https://doi.org/10.1073/pnas.1509453112.
[11] A.P. Raman, M.A. Anoma, L. Zhu, E. Rephaeli, S. Fan, Passive radiative cooling below ambient air temperature under direct sunlight, Nature 515 (2014) 540–544, https://doi.org/10.1038/nature13883.
[12] A. Deinega, I. Valuev, B. Potapkin, Y. Lozovik, Minimizing light reflection from dielectric textured surfaces, J. Opt. Soc. Am. A. 28 (2011) 770, https://doi.org/10.1364/josaa.28.000770.
[13] D.Z. Dimitrov, C.-H. Du, Crystalline silicon solar cells with micro/nano texture, Appl. Surf. Sci. 266 (2013) 1–4, https://doi.org/10.1016/J.APSUSC.2012.10.081.
[14] J. Van De Groep, P. Spinelli, A. Polman, Single-step soft-imprinted large-area nanopatterned antireflection coating, Nano Lett. 15 (2015) 4223–4228, https://doi.org/10.1021/acs.nanolett.5b01623.
[15] M.G. Deceglie, V.E. Ferry, A.P. Alivisatos, H.A. Atwater, Design of nanostructured solar cells using coupled optical and electrical modeling, Nano Lett. 12 (2012) 2894–2900, https://doi.org/10.1021/nl300483y.
[16] S. Dominguez, I. Cornago, J. Bravo, J. Pérez-Conde, H.J. Choi, J.-G. Kim, G. Barbastathis, Simple fabrication of ultrahigh aspect ratio nanostructures for enhanced antireflectivity, J. Vac. Sci. Technol. B, Nanotechnol. Microelectron. Mater. Process. Meas. Phenom. 32 (2014), 030602, https://doi.org/10.1116/1.4869302.
[17] Q. Chen, G. Hubbard, P.A. Shields, C. Liu, D.W.E. Allsopp, W.N. Wang, S. Abbott, Broadband moth-eye antireflection coatings fabricated by low-cost nanoimprinting, Appl. Phys. Lett. 94 (2009), 263118, https://doi.org/10.1063/1.3171930.
[18] C.-Y. Lin, K.-Y.A. Lin, T.-W. Yang, Y.-C. Chen, H. Yang, Self-assembled hemispherical nanowell arrays for superhydrophobic antireflection coatings, J. Colloid Interface Sci. 490 (2017) 174–180, https://doi.org/10.1016/J.JCIS.2016.11.064.
[19] M. Clemens, T. Weil, Discrete electromagnetism with the finite integration technique, Prog. Electromagn. Res. 32 (2001) 65–87, https://doi.org/10.2528/PIER00080103.
[20] Sagrario Domínguez Fernández, Design and Fabrication of Nanostructures for Enhanced Ligth Absorption in Silicon, Universidad Pública de Navarra, 2015.
[21] C. Kenneth, Johnson, GD-Calc, 2005. https://kjinnovation.com/.
[22] M.G. Moharam, T.K. Gaylord, Rigorous Coupled-Wave Analysis of Planar-Grating Diffraction, J. Opt. Soc. Am. 71 (1981) 811. https://doi.org/10.1364/JOSA.71.000811.
[23] J. Gjessing, Photonic Crystals for Light Trapping in Solar Cells, University of Oslo, 2011, p. 164. https://www.uio.no/studier/emner/matnat/its/TEK5400/h19/TEK%205400%20H2019/papers/gjessing_phd_thesis_submitted28oct2011.pdf.
[24] M. Rubin, Optical properties of soda lime silica glasses, Sol. Energy Mater. 12 (1985) 275–288, https://doi.org/10.1016/0165-1633(85)90052-8.
[25] M.N. (Manindra N. Das, N.C. Giri, Design and Analysis of Experiments, New Age International, 2006. https://www.google.com/books/edition/Design_and_Analysis_of_Experiments/-vGlnx-ZVvEC?hl=en&gbpv=0. (Accessed 12 November 2020).
[26] M.M. Hossain, M. Gu, Radiative cooling: principles, progress, and potentials, Adv. Sci. 3 (2016) 1–10, https://doi.org/10.1002/advs.201500360.
[27] Gemini Observatory, IR Transmission Spectra, (n.d.). http://www.gemini.edu/?q=node/10789. (Accessed 29 October 2020).
[28] N.R.E. Laboratory, Spectral solar irradiance, SMARTS: simple model of the atmospheric radiative transfer of sunshine., (n.d.). https://www.nrel.gov/grid/solar-resource/smarts.html. (Accessed 29 October 2020).
[29] M. Clyde, Creveling, Tolerance Design: A Handbook for Developing Optimal Specifications, Addison-Wesley Educational Publishers Inc, 1997, 20 December 1996, https://www.amazon.ae/Tolerance-Design-Handbook-Developing-Specifications/dp/0201634732.